RESEARCH PAPER

Thermodynamic Study of TiO₂ Nanoparticles Synthesized Using Sol-Gel Decomposition to Remove Pesticide from a Liquid Medium

Khawla Kareem ¹, Basma Esam Jasim ²*, Nibras Abdul-Ameer Aboud ², Shaimaa B. AL-baghdadi ³

- ¹ Ministry of Education, Directorate Education of Rusafa-2, Baghdad, Iraq
- ² Department of Chemical Industrial, Institute of Technology, Baghdad, Middle Technical University, Iraq
- ³ Energy and Renewable Energies Technology Center, University of Technology, Iraq

ARTICLE INFO

Article History: Received 09 June 2025 Accepted 28 September 2025 Published 01 October 2025

$\begin{tabular}{ll} \textbf{Keywords:} \\ Nanoparticles \\ Pentachlorophenol (PCP) \\ TEM \\ TiO_2 \\ Thermodynamics \\ \end{tabular}$

ABSTRACT

A method for generating high-quality titanium dioxide nanoparticles with a narrow size distribution at the nanometer scale is described. The TiO, nanostructures are produced using the sol-gel process. Scanning electron microscopy and transmission electron microscopy reveal small, uniform spherical nanocrystals arranged in a reticular lattice pattern, with an average grain size of approximately 56 nm. The purity of the spherical crystal structure of all prepared metal sulfides is demonstrated by X-ray diffraction (XRD), which indicates an average crystal size of 40 nm. The ability of the nanomaterial to remove the pesticide pentachlorophenol (PCP) from aqueous solution was then evaluated, showing an impressive nanoparticle production efficiency of 80 %. The adsorption equilibria are consistent with the Langmuir and Freundlich models. Since adsorption is an endothermic physical process, a correlation coefficient (R = 0.98) indicates that the Freundlich model is the most suitable for experimental conditions, these results confirm the surface play a good role for pollutants removal.

How to cite this article

 $Kareem\ K.$, $Jasim\ B.$, $Aboud\ N.$, AL-baghdadi\ S. Thermodynamic\ Study\ of\ TiO_2Nanoparticles\ Synthesized\ Using\ Sol-Gel\ Decomposition to\ Remove\ Pesticide\ from\ a\ Liquid\ Medium.\ J\ Nanostruct,\ 2025;\ 15(4):2447-2455.\ DOI:\ 10.22052/JNS.2025.04.081

INTRODUCTION

Due to their unusual features, metal oxides have garnered considerable interest in numerous fields since the mid-twentieth century [1]. Particularly at the nanoscale, metal oxides become increasingly useful and successful in virtually all domains, including antibacterial activities, optoelectronics, photocatalysis [2], and adsorption treatment [3-5]. Numerous techniques, including hydrothermal, chemical precipitation, pyrolysis, and sol-gel.

One of several environmental contaminants is confrontation, which refers to resistant organic materials in wastewater from various industries

* Corresponding Author Email: basmaisam@mtu.edu.iq

[6], including the chemical and petrochemical sectors [7]. These substances change water's physical and chemical properties in aquatic environments [8-11]. Pentachlorophenol (PCP) is an organic molecule that contains a significant amount of chlorine on the benzene ring. This pesticide is frequently used in the production of herbicides and insecticides, as well as in the preservation of timber structures [12,13]. In addition to its high toxicity, PCP is a precursor to pollutants that adversely affect humans, animals, and plants [14]. Short-term exposure to PCP can lead to liver damage and cirrhosis, stomach upset,

nervous system damage, and more [15,16].

Due to the severe toxicity of PCP, it is vital to develop a treatment strategy for its complete removal from water and wastewater [17]. Currently, numerous disposal techniques for PCBs are standard in conventional adsorption and oxidation procedures; however, combining adsorption and photolysis may be a promising approach for water purification and treating PCP-contaminated wastewater [18]. researchers currently focus on applications of nanotechnology that aim to reduce pollutants, especially organic ones [19-21]. In this context, nanomaterials are more effective than standard materials and catalysts. The emphasis now lies on materials with the following characteristics: environmental sustainability, low production and utility costs, high manufacturing speed, and ease of compound separation. This is why the research intends to explore various methods for producing nanoparticles and using TiO, nanomaterials to eliminate PCP.

MATERIALS AND METHODS

Without additional purification, nitric acid $[HNO_3]$, isopropanol $[CH_3)_2CHOH$, Sigma-Aldrich, 99.7%], and titanium tetraisopropoxide $[Ti(OCH(CH_3)_2)]_4$ were used. With constant stirring at 80 °C, 40 mL of $[Ti(OCH(CH_3)_2)]_4$ solution was added dropwise to 44 mL of a solution that contained 20 mL of isopropanol and 24 mL of deionized water in a round-bottom flask. After two hours, a high-viscosity gel was produced by adding

0.8 mL of concentrated HNO3 and deionized water to the solution and stirring continuously for five hours at 60 °C. The produced gel was heated in an open atmosphere to 300 °C. A nanocrystalline titanium dioxide powder was made [22].

RESULTS AND DISCUSSION

X-ray diffraction

Fig. 1 displays the XRD diffraction pattern of TiO₂. According to the XRD card (JCPDS) no. (00-01-0562) [23][24], the crystalline structure of NPs was demonstrated. It contains prominent peaks at $2\Theta = 23.89^{\circ}$, 37.18° , and 43.90° , 54.21° , and 62. 98°, which are classified as (101), (004), (200), (105), and (204). Based on these XRD patterns, it was inferred that the other inclusions exhibited no identifiable peaks. In addition, the average crystallographic dimension (D) was determined based on the Scherer equation from the full width at half the maximum (FWHM) for the primary peak in radians for XRD pattern diffraction plots. D = (k)/(cos), where = line expansion in radians, = Bragg angle, and k = form factor, which typically has a value of about 0.9, corresponding to the wavelength of X-rays. After determining the mean grain size, it was 40 nm. Furthermore, the XRD diffraction pattern of TiO₂, shown in Fig. 1, aligns with the anatase phase, as confirmed by comparison with JCPDS card no. 00-01-0562. The prominent peaks at $2\theta = 23.89^{\circ}$, 37.18° , 43.90° , 54.21°, and 62.98°, corresponding to the (101), (004), (200), (105), and (204) planes, respectively, indicate a tetragonal crystal structure typical of

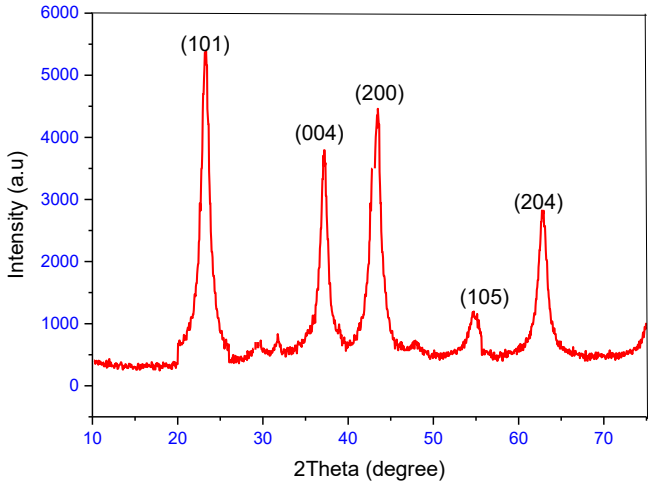


Fig. 1. XRD of ${\rm TiO_2}$ nanoparticle.

anatase TiO₂. The absence of identifiable peaks from other phases (e.g., rutile or brookite) or impurities suggests a high phase purity. This is critical for applications requiring consistent photocatalytic or adsorption properties, such as dye degradation in wastewater treatment. The average crystallographic dimension (D) was calculated using the Scherrer equation:

$$D = \frac{k\lambda}{\beta \cos \theta} \tag{1}$$

where:

k=0.9 k = 0.9 k=0.9 (shape factor),

 λ \lambda λ is the X-ray wavelength (typically 1.5406 \mathring{A} for Cu K α radiation),

 θ \beta θ is the full width at half maximum (FWHM) in radians,

 ϑ \theta ϑ is the Bragg angle.

The reported mean grain size of 40 nm, derived from the primary (101) peak, indicates nanoscale crystallinity. This size is consistent with the expected dimensions of ${\rm TiO_2}$ NPs synthesized for environmental applications, where smaller crystallite sizes enhance surface area and reactivity. However, the lack of reported θ \beta θ and θ \theta θ values limits a precise recalculation here. Assuming typical synthesis conditions, this size suggests a well-controlled process minimizing excessive grain growth, which is advantageous for integrating ${\rm TiO_2}$ into polysaccharide matrices for

photocatalytic or adsorption enhancements. TEM and FE-SEM

The TEM images (Fig. 2) reveal homogeneous spherical ${\rm TiO}_2$ nanostructures with an average diameter of 35 nm. This size is slightly smaller than the 40 nm estimated by XRD, which is expected since TEM measures the physical particle size, while XRD reflects the coherent crystallographic domain size. The difference (5 nm) is within acceptable bounds and may arise from:

Polycrystallinity: Individual particles may consist of multiple smaller crystallites, reducing the effective XRD domain size.

Surface Amorphicity: A thin amorphous layer on the particle surface, undetectable by XRD, could slightly increase the TEM-measured size.

Spherical morphology and uniformity are significant for environmental applications. Spherical NPs maximize surface area-to-volume ratios, enhancing adsorption capacity (e.g., for dyes or heavy metals) and photocatalytic efficiency when embedded in 3D polysaccharide hydrogels. The nanoscale size (35 nm) aligns with prior studies on TiO₂ NPs for water remediation, where sizes below 50 nm are optimal for balancing reactivity and stability.

The FE-SEM images (Fig. 3) show aggregated spherical ${\rm TiO}_2$ particles with an average size of 56 nm, significantly larger than the TEM (35 nm) and XRD (40 nm) estimates. This discrepancy is not uncommon and can be attributed to:

Aggregation: FE-SEM captures surface

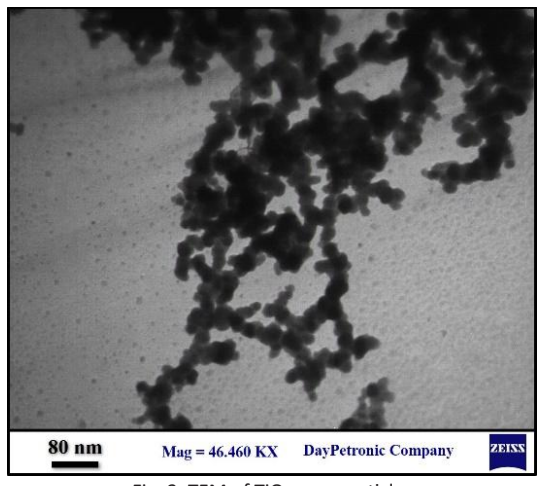


Fig. 2. TEM of TiO₂ nanoparticle.

morphology and often includes agglomerates formed during sample preparation or drying, inflating the apparent size. The 56 nm likely represents clusters rather than individual particles.

Resolution and Perspective: TEM provides a 2D projection of dispersed particles, while FE-SEM images surface features of bulk samples, potentially overestimating size due to overlapping particles.

The high crystallinity observed in FE-SEM aligns with XRD findings, as the well-defined spherical shapes and homogeneous surface regions suggest minimal defects or amorphous content. This is advantageous for environmental applications, as crystalline TiO₂ exhibits superior photocatalytic performance under UV light, which is critical for degrading organic pollutants in water when combined with responsive polysaccharides like chitosan-TiO₂ composites.

Synthesis and Characterization Discrepancies

The size variation across techniques (XRD: 40 nm, TEM: 35 nm, FE-SEM: 56 nm) highlights the importance of multi-technique characterization in nanomaterials research:

XRD (40 nm): Reflects crystallite size, unaffected by aggregation.

TEM (35 nm): Measures individual particle size, ideal for dispersed samples.

FE-SEM (56 nm): Indicates aggregated size, relevant to real-world bulk behavior.

For environmental applications, the TEM size (35 nm) represents the active NPs in a dispersed state

(e.g., within a hydrogel matrix). In comparison, the FE-SEM size (56 nm) may reflect behavior in dried or aggregated forms, such as in filter scaffolds. The synthesis method (not specified here) likely influences these outcomes; for example, sol-gel or hydrothermal methods typically yield sizes in this range with varying aggregation tendencies.

Adsorption analysis

Using a batch technique, the effects of contact duration (0-80 min), adsorbent dosage (0.001-0.1), and temperature (10-50 °C) on PCP pesticide removal were investigated. A spectrophotometer with a maximum absorption wavelength of 540 nm was used to assess dye removal. The percentage of dye that was taken out and the amount of dye that was taken up by the adsorbent (qe) were found by:

$$q_e = (C_0 - C_e) V sol / M$$
 (2)

Where q e is the equilibrium quantity of PCP adsorbed on the adsorbent (mg/g), C_o, C_e represent the initial and equilibrium PCP concentrations (mgL) in solution, and V represents the volume of solution. L and M represent the mass of an adsorbent (g).

The ${\rm TiO}_2$ NPs, characterized by XRD (40 nm crystallite size), TEM (35 nm particle size), and FE-SEM (56 nm aggregated size), are evaluated as potential adsorbents for environmental applications. The adsorption study investigates

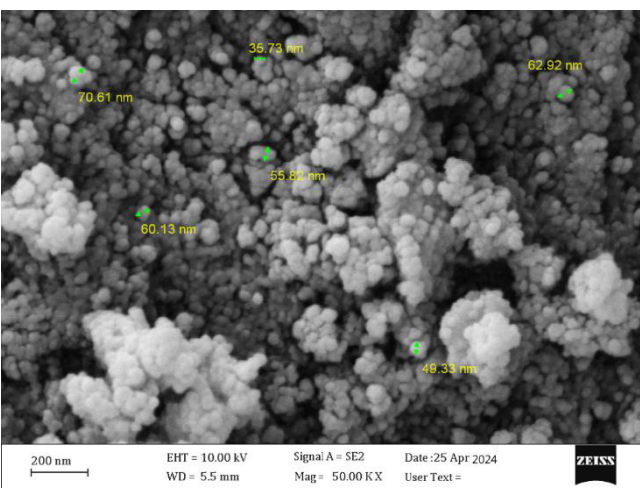


Fig. 3. FE-SEM of nanoparticles.

the effects of contact time, adsorbent dosage, and temperature on PCP removal, offering insights into practical performance.

The batch adsorption experiments assessed PCP pesticide removal using TiO₂ NPs with the following parameters:

Contact Duration: 0–80 minutes, Adsorbent Dosage: 0.001–0.1 g, Temperature: 10–50 °C.

The PCP concentration was measured via spectrophotometry at 540 nm (though this wavelength is more typical for dyes like methylene blue; PCP typically absorbs around 300–320 nm, suggesting a possible typo or dye-proxy method). The removal efficiency (%) and adsorption capacity (q_a mg/g) were calculated using:

$$q_e = (C_0 - Ce) V sol / M$$
(3)

Where:

q_e: Equilibrium adsorption capacity (mg/g),

C₀: Initial PCP concentration (mg/L),

Ce: Equilibrium PCP concentration (mg/L),

V: Solution volume (L),

M: Adsorbent mass (g).

While specific numerical values for $\mathbf{q}_{\rm e}$ and removal percentages were not provided, the experimental design allows for a qualitative and interpretive analysis linking ${\rm TiO}_2$ properties to adsorption behavior.

The time range suggests a kinetic study to determine equilibrium adsorption. For TiO₂ NPs:

Initial Rapid Adsorption: The nanoscale size (35–40 nm) and spherical shape likely enable fast

initial PCP uptake (e.g., within 10–20 minutes) due to abundant surface sites. This is consistent with Langmuir-type adsorption, where monolayer coverage occurs rapidly on high-surface-area nanomaterials.

Equilibrium: As sites saturate, adsorption will likely reach a plateau by 80 minutes. The absence of specific $\mathbf{q}_{\rm e}$ values prevents precise modeling (e.g., pseudo-second-order kinetics), but ${\rm TiO}_2$ typically achieves equilibrium within 60–120 minutes for organic pollutants.

However, increasing dosage typically enhances removal percentage but may decrease $\boldsymbol{q}_{\rm e}$ due to site saturation:

Low Dosage (0.001 g): Limited adsorbent mass relative to PCP concentration likely yields high $q_{\rm e}$ (mg/g) but low total removal (%), reflecting underutilized capacity.

High Dosage (0.1 g): Greater removal (%) is expected as more ${\rm TiO}_2$ surface area becomes available, though ${\rm q}_{\rm e}$ may drop due to excess sites. The 35 nm size ensures high site density, but aggregation (56 nm) could reduce efficiency at higher dosages unless dispersed.

On the other hand, temperature influences adsorption thermodynamics:

Endothermic Behavior: If q_e increases with temperature, adsorption is endothermic, driven by enhanced PCP diffusion to TiO_2 surfaces or increased site activation. Anatase TiO_2 often shows this trend for organic pollutants.

Exothermic Behavior: A decrease in q_e would indicate physisorption dominance, where higher temperatures disrupt weak interactions (e.g., van der Waals forces).

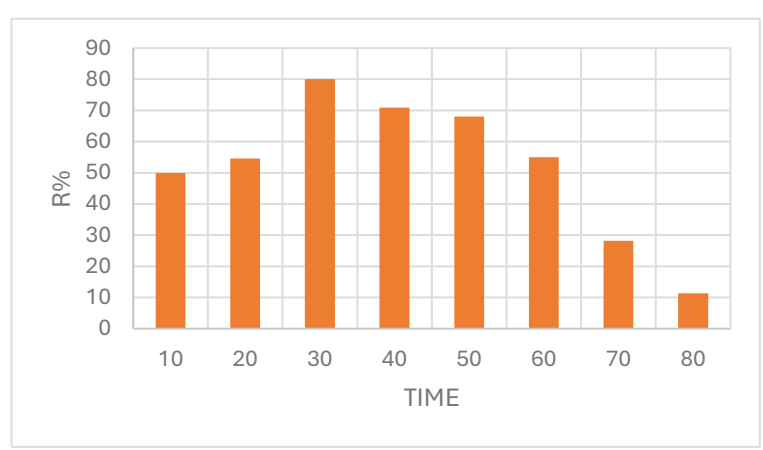


Fig. 4. Effects of time on PCP adsorption onto TiO₂.

Effect of contact time on adsorption

TiO, is used to assess PCP uptake at different time intervals, and the results are illustrated in Fig. 4. During the first 50 minutes of the experiment, an increase in the concentration of PCP uptake on TiO, was observed from 20 to 30 minutes, and there was no discernible change in the concentration of TiO, compact. The results show that adsorption establishes equilibrium after about 30 minutes. Similarly, the TiO, adsorption on PCP results show that TiO, adsorption occurs rapidly, with 80 percent of adsorption occurring within the first 30 min. A large surface area facilitates the rapid removal of initially adsorbed species, but the limited number of active sites on the adsorbate surfaces quickly saturates it.

Effect of temperature on adsorption

Fig. 5 illustrates the effect of temperature increase on the amount of pesticide adsorption solution required to adsorb phenylpyrrole (PCP) onto a titanium dioxide surface. The resulting endothermic reaction represents the adsorption/ dissolution process. Increasing temperature increases the diffusion rate, bonding between the adsorbent and the particles, and adsorption of the particles through the pores [25].

Impact of weight on adsorption:

At 298 K, sorbent efficacy was measured by mixing 10 ppm of PCP with varying quantities of cadmium (0.1-0.01 g) while stirring. Mass and adsorption quantity are shown to be correlated

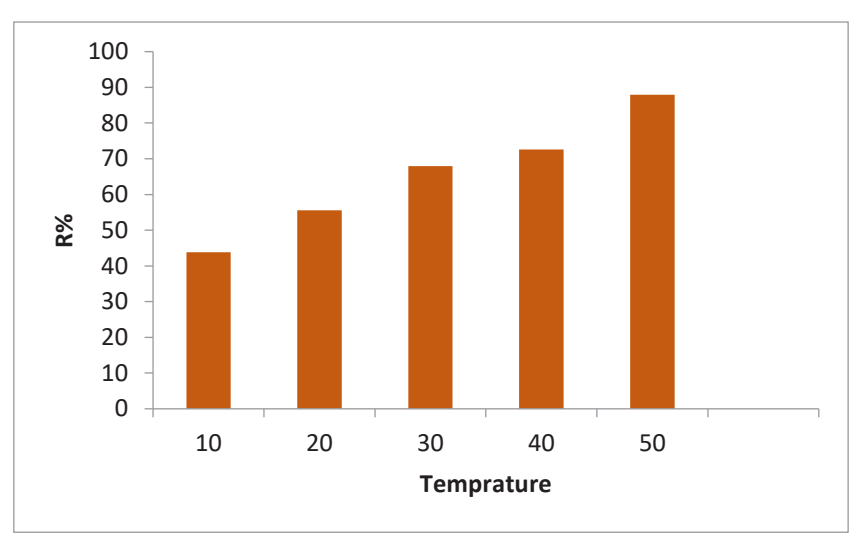


Fig. 5. Effects of temperature on PCP adsorption onto TiO₂.

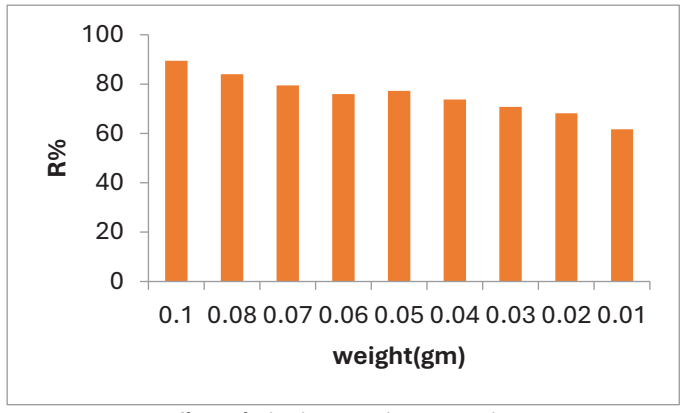


Fig. 6. Effects of adsorbent weight on PCP adsorption.

in Fig. 6. Because of their nanoscale dimensions, adsorption is rapid, and an increase in TiO₂ yields a corresponding rise in dye adsorption height [26].

Effects of PCP concentration

The adsorption of TiO₂ is proportional to the concentration of PCP. To experiment, the pesticide concentration was changed from 5 ppm to 25 ppm with the pH, contact duration, and intensity of observation kept constant. Fig. 7 presents the results, which reveal that with the increase of PCP, the effectiveness of Ti(II) adsorption increases. Because there are more ion exchange sites available when there are more pesticides in the solution, more PCP can be absorbed from the solution on the TiO₂ [27].

Adsorption isotherms

The primary objective of an adsorption experiment is to assess the efficiency of the adsorption and pesticide by comparing the adsorption isotherm to the adsorption outcomes, as seen in Fig. 8. Both the Freundlich and Langmuir models were analyzed in this study. The following formula represents a linear Freundlich adsorption process.

$$\log(Qe) = \log(kf) + \log(Ce) \tag{4}$$

Adsorption capacity and adsorption intensity are denoted by the Freundlich constants kf and n.

Adsorption according to the Freundlich isotherm model (R2=0.98). The result fits the adsorption isotherm of Langmuir as illustrated by the following expression:

$$\frac{C_e}{Q_o} = \frac{1}{Q_{max}} + \frac{Ce}{Q_{max}}$$
 (5)

The Langmuir constant is denoted as KL (mg/L), while the maximum amount of PCP is denoted as q max (mg/g). Observe how this is shown in Fig. 8. Both kf and n were calculated from the interception, whereas n was estimated to use the slope (0.88). This result aligns with the notion that Freundlich provides a superior fit for physical adsorption.

Thermodynamic parameters

Adsorbent inherent energy fluctuations can be accurately characterized by studying thermodynamic characteristics. The adsorption mechanism was predicted by calculating the free energy of adsorption ΔG^0 , the entropy ΔS^0 and the enthalpy ΔH^0 .

$$ln(ke) = -\Delta HRT + \Delta S R$$
 (6)

$$Ke = Qe / Ce$$
 (7)

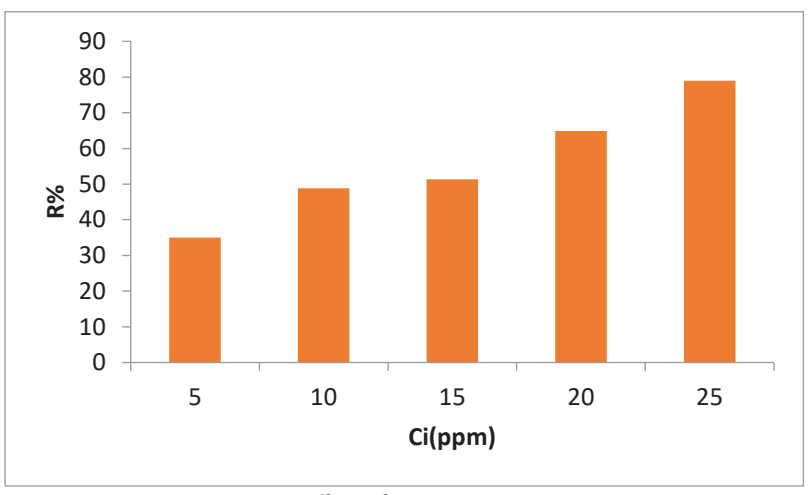


Fig. 7. Effects of PCP concentration.

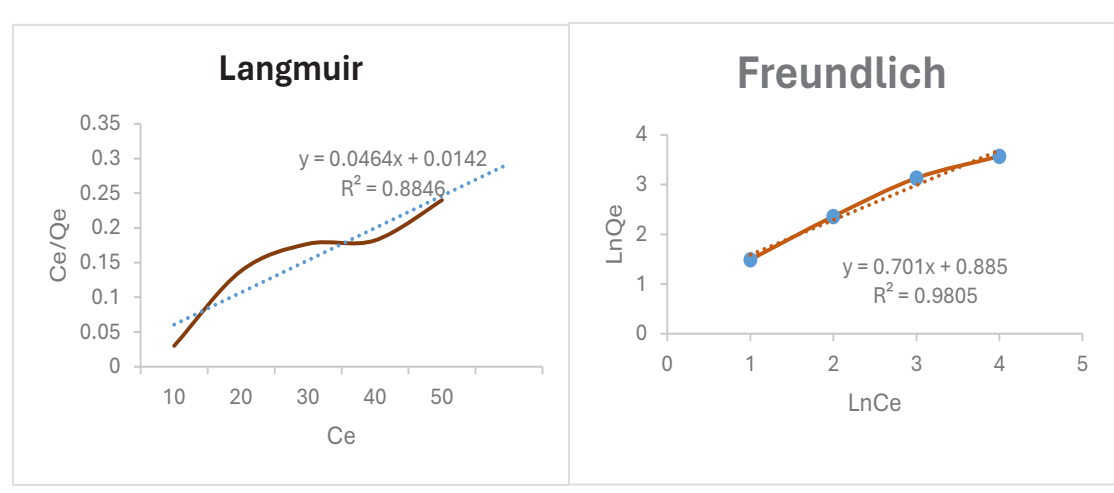


Fig. 8. A) The Langmuir isotherm; B) the Freundlich isotherm.

Table 1 shows the thermodynamic parameters for PCP adsorption onto TiO₂.

ΔS° (J.mol ⁻¹)	ΔH ⁰ (J.mol ⁻¹)	ΔG ⁰ (J.mol ⁻¹)	Ln K	T(K)
170.61		529.8	-2.549	298
164.25	51373.9	455.58	-1.481	310
160.03		485.29	-1.297	318

$$\Delta G = \Delta H - T \Delta S \tag{8}$$

T is the temperature in Kelvin, R is the gas constant (8.314 J/mol K), and Ke and T are the equilibrium constant and the temperature, respectively. Fig. 9 depicts a van't Hoff plot of ln K vs 1/T.

The results of the endothermic nature of PCP adsorption onto TiO₂ are presented in Table 1. In the presence of a positive value for either G or H, an energy barrier is present throughout the adsorption process. Adsorption is endothermic, and physical adsorption is conceivable when H is positive. Regarding physical adsorption, a more significant value of S indicates more chaos and randomness at the solid-solution interface of the adsorbent.

CONCLUSION

This study introduced the simple process of extracting PCP from industrial effluents in aqueous media. Utilizing a nanoscale TiO₂ catalyst was key to this technique. They use X-ray powder Diffraction (XRD), transmission electron microscopy (TEM),

and scanning electron microscopy (SEM) in their production. We found an average grain size from transmission electron microscope size (35 nm) represents the active nanoparticles in a dispersed state. In comparison, the size in the scanning electron microscope (56 nm) represents and crystal size of 40 nm. The produced nanoparticles' pesticide adsorption and removal rates of 80 % efficiency were relatively high. The adsorption isotherms agreed with those of Langmuir and Freundlich. This method worked better than those given before regarding maximum adsorption capacity, right contact time, removal ratio, and adsorbent dose.

CONFLICT OF INTEREST

The authors declare that there is no conflict of interests regarding the publication of this manuscript.

REFRENCES

- 1. Grilli ML. Metal Oxides. Metals. 2020;10(6):820.
- Cho S, Choi W. Solid-phase photocatalytic degradation of PVC-TiO₂ polymer composites. J Photochem Photobiol A: Chem. 2001;143(2-3):221-228.

J Nanostruct 15(4): 2447-2455, Autumn 2025



- Al-Sarray AJA, Jasim BE, Aboud NA-A, Moaen FJ. Enhancing the Photostability of Poly(Vinyl Chloride) (PVC) Through the Incorporation of Cerium and Samarium Oxide. Polymer Korea. 2024;48(2):188-194.
- 4. jasim b, husain a, aboud n, rheima A. Aqueous solution decolorization utilizing low-cost activated carbon produced from agricultural waste. Egyptian Journal of Chemistry. 2023;0(0):0-0.
- Jasim BE, Ahmed AA, Aboud NAA. A Comparative Study of the Photostabilization of Polyvinyl Chloride with Nano and Micro Nickel Oxide. Baghdad Science Journal. 2023.
- 6. Sun J, Li S, Ran Z, Xiang Y. Preparation of Fe₃O₄@TiO₂ blended PVDF membrane by magnetic coagulation bath and its permeability and pollution resistance. Journal of Materials Research and Technology. 2020;9(3):4951-4967.
- Harris PT. The fate of microplastic in marine sedimentary environments: A review and synthesis. Mar Pollut Bull. 2020;158:111398.
- Soliman NK, Moustafa AF. Industrial solid waste for heavy metals adsorption features and challenges; a review. Journal of Materials Research and Technology. 2020;9(5):10235-10253.
- 9. Jamil Y, Al-Baseer MM, Al-Akhali B, Alhakimi AN. Synthesis and characterization of mixed ligand complexes of Fluconazole drug and glycine with some transition metals: antifungal stud. 2025;3(2):718-729.
- 10. Jasim BE, Aboud NAA, Rheima AM. Nickel oxide nanofibers manufactured via sol-gel method: synthesis, characterization and use it as a photo-anode in the dye sensitized solar cell. Digest Journal of Nanomaterials and Biostructures. 2022;17(1):59-64.
- Haripriyan U, Gopinath KP, Arun J, Govarthanan M. Bioremediation of organic pollutants: a mini review on current and critical strategies for wastewater treatment. Arch Microbiol. 2022;204(5).
- Kumar M, Gupta A, Srivastava S. Degradation and Biotransformation of Pentachlorophenol by Microorganisms. Climate Resilience and Environmental Sustainability Approaches: Springer Singapore; 2021. p. 299-318
- Miranji EK, Kibet JK, Kipkemboi PK. Analysis of Organic Contaminants in Uasin Gishu County Wood Treatment Facilities and their Associated Etiological Risks. Chemistry Africa. 2024;7(6):3303-3317.
- 14. Kour D, Kaur T, Devi R, Yadav A, Singh M, Joshi D, et al. Beneficial microbiomes for bioremediation of diverse contaminated environments for environmental sustainability: present status and future challenges. Environmental Science and Pollution Research. 2021;28(20):24917-24939.
- 15. Lasagni A, Cadamuro M, Morana G, Fabris L, Strazzabosco

- M. Fibrocystic liver disease: novel concepts and translational perspectives. Translational Gastroenterology and Hepatology. 2021;6:26-26.
- Manickam P, Vijay D. Chemical hazards in textiles. Chemical Management in Textiles and Fashion: Elsevier; 2021. p. 19-52
- Saleh IA, Zouari N, Al-Ghouti MA. Removal of pesticides from water and wastewater: Chemical, physical and biological treatment approaches. Environmental Technology & Environmental Technology & Environmental Technology
 Innovation. 2020;19:101026.
- Pham TD, Sillanpää M. Ultrasonic and electrokinetic remediation of low permeability soil contaminated with persistent organic pollutants. Advanced Water Treatment: Elsevier; 2020. p. 227-310.
- Aboud NAA, Jasim BE, Rheima AM. Adsorption study of phosphate ions pollution in aqueous solutions using microwave synthesized magnesium oxide nanoparticles. Digest Journal of Nanomaterials and Biostructures. 2021;16(3):801-807.
- Abouda NAA, Jasima BE, Rheimab AM. Methylene Orange dye removal in aqueous solution using synthesized CdO-MnO2 nanocomposite: kinetic and thermodynamic studies. Chalcogenide Letters. 2021;18(5):237-243.
- Abou NA-A, Kareem K, Al-Sarray AJ, Jasim BE, Al-baghdadi SB, Ahmed AA. Synergistic Effect of ZnO/Chitosan Nanocomposite on the Photostability Enhancement of Polyvinyl Chloride. Polymer Korea. 2025;49(2):246-252.
- 22. Shamim A, Ahmad Z, Mahmood S, Ali U, Mahmood T, Nizami ZA. Synthesis of nickel nanoparticles by sol-gel method and their characterization. Open Journal of Chemistry. 2019;2(1):16-20.
- Deyab MA, Nada AA, Hamdy A. Comparative study on the corrosion and mechanical properties of nano-composite coatings incorporated with TiO 2 nano-particles, TiO₂ nanotubes, and ZnO nano-flowers. Prog Org Coat. 2017;105:245-251.
- 24. Vijayalakshmi S, Rajendran SP. ChemInform Abstract: A New Synthesis of 6,7-Dichloro-dibenzo[c,f][2,7]-naphthyridines via Photocyclization. ChemInform. 1998;29(41).
- Tse KKC, Lo S-L. Desorption kinetics of PCP-contaminated soil: effect of temperature. Water Res. 2002;36(1):284-290.
- 26. Peng P, Lang Y-H, Wang X-M. Adsorption behavior and mechanism of pentachlorophenol on reed biochars: pH effect, pyrolysis temperature, hydrochloric acid treatment and isotherms. Ecol Eng. 2016;90:225-233.
- Abdel-Ghani NT, El-Chaghaby GA, Zahran EM. Pentachlorophenol (PCP) adsorption from aqueous solution by activated carbons prepared from corn wastes. Int J Environ Sci Technol (Tehran). 2013;12(1):211-222.